

Northumbria Research Link

Citation: Elmarakbi, Ahmed (2011) Finite Element Analysis of Delamination Growth in Composite Materials using LS-DYNA: Formulation and implementation of new cohesive elements. In: Advances in Composite Materials: Ecodesign and Analysis. Intechopen, pp. 409-428. ISBN 978-953-307-150-3

Published by: Intechopen

URL:

This version was downloaded from Northumbria Research Link:
<http://nrl.northumbria.ac.uk/id/eprint/37342/>

Northumbria University has developed Northumbria Research Link (NRL) to enable users to access the University's research output. Copyright © and moral rights for items on NRL are retained by the individual author(s) and/or other copyright owners. Single copies of full items can be reproduced, displayed or performed, and given to third parties in any format or medium for personal research or study, educational, or not-for-profit purposes without prior permission or charge, provided the authors, title and full bibliographic details are given, as well as a hyperlink and/or URL to the original metadata page. The content must not be changed in any way. Full items must not be sold commercially in any format or medium without formal permission of the copyright holder. The full policy is available online: <http://nrl.northumbria.ac.uk/policies.html>

This document may differ from the final, published version of the research and has been made available online in accordance with publisher policies. To read and/or cite from the published version of the research, please visit the publisher's website (a subscription may be required.)

Finite Element Analysis of Delamination Growth in Composite Materials using LS-DYNA: Formulation and Implementation of New Cohesive Elements

Ahmed Elmarakbi

*Faculty of Applied Sciences, University of Sunderland
United Kingdom*

1. Introduction

This chapter provides an overview of the delamination growth in composite materials, cohesive interface models and finite element techniques used to simulate the interface elements. For completeness, the development and implementation of a new constitutive formula that stabilize the simulations and overcome numerical instabilities will be discussed in this chapter.

Delamination is a mode of failure of laminated composite materials when subjected to transverse loads. It can cause a significant reduction in the compressive load-carrying capacity of a structure. Cohesive elements are widely used, in both forms of continuous interface elements and point cohesive elements, (Cui & Wisnom, 1993; De Moura et al., 1997; Reddy et al., 1997; Petrossian & Wisnom, 1998; Shahwan & Waas, 1997; Chen et al., 1999; Camanho et al., 2001) at the interface between solid finite elements to predict and to understand the damage behaviour in the interfaces of different layers in composite laminates. Many models have been introduced including: perfectly plastic, linear softening, progressive softening, and regressive softening (Camanho & Davila, 2004). Several rate-dependent models have also been introduced (Glennie, 1971; Xu et al., 1991; Tvergaard & Hutchinson, 1996; Costanzo & Walton, 1997; Kubair et al., 2003). A rate-dependent cohesive zone model was first introduced by Glennie (Glennie, 1971), where the traction in the cohesive zone is a function of the crack opening displacement time derivative. Xu et al. (Xu et al., 1991) extended this model by adding a linearly decaying damage law. In each model the viscosity parameter (η) is used to vary the degree of rate dependence. Kubair et al. (Kubair et al., 2003) thoroughly summarized the evolution of these rate-dependant models and provided the solution to the mode III steady-state crack growth problem as well as spontaneous propagation conditions.

A main advantage of the use of cohesive elements is the capability to predict both onset and propagation of delamination without previous knowledge of the crack location and propagation direction. However, when using cohesive elements to simulate interface damage propagations, such as delamination propagation, there are two main problems. The first one is the numerical instability problem as pointed out by Mi et al. (Mi et al., 1998), Goncalves et al. (Goncalves et al., 2000), Gao and Bower (Gao & Bower, 2004) and Hu et al.

(Hu et al., 2007). This problem is caused by a well-known elastic snap-back instability, which occurs just after the stress reaches the peak strength of the interface. Especially for those interfaces with high strength and high initial stiffness, this problem becomes more obvious when using comparatively coarse meshes (Hu et al., 2007). Traditionally, this problem can be controlled using some direct techniques. For instance, a very fine mesh can alleviate this numerical instability, however, which leads to very high computational cost. Also, very low interface strength and the initial interface stiffness in the whole cohesive area can partially remove this convergence problem, which, however, lead to the lower slope of loading history in the loading stage before the happening of damages. Furthermore, various generally oriented methodologies can be used to remove this numerical instability, e.g. Riks method (Riks, 1979) which can follow the equilibrium path after instability. Also, Gustafson and Waas (Gustafson & Waas, 2008) have used a discrete cohesive zone method finite element to evaluate traction law efficiency and robustness in predicting decohesion in a finite element model. They provided a sinusoidal traction law which found to be robust and efficient due to the elimination of the stiffness discontinuities associated with the generalized trapezoidal traction law.

Recently, the artificial damping method with additional energy dissipations has been proposed by Gao and Bower (Gao & Bower, 2004). Also, Hu et al. proposed a kind of move-limit method (Hu et al., 2007) to remove the numerical instability using cohesive model for delamination propagation. In this technique, the move-limit in the cohesive zone provided by artificial rigid walls is built up to restrict the displacement increments of nodes in the cohesive zone of laminates after delaminations occurred. Therefore, similar to the artificial damping method (Gao & Bower, 2004), the move-limit method introduces the artificial external work to stabilize the computational process. As shown later, although these methods (Gao & Bower, 2004; Hu et al., 2007) can remove the numerical instability when using comparatively coarse meshes, the second problem occurs, which is the error of peak load in the load-displacement curve. The numerical peak load is usually higher than the real one as observed by Goncalves et al. (Goncalves et al., 2000) and Hu et al. (Hu et al., 2007).

Similar work has also been conducted by De Xie and Waas (De Xie & Waas, 2006). They have implemented discrete cohesive zone model (DCZM) using the finite element (FE) method to simulate fracture initiation and subsequent growth when material non-linear effects are significant. In their work, they used the nodal forces of the rod elements to remove the mesh size effect, dealt with a 2D study and did not consider viscosity parameter. However, in the presented Chapter, the author used the interface stiffness and strength in a continuum element, tackled a full 3D study and considered the viscosity parameter in their model.

With the previous background in mind, the objective of this Chapter is to propose a new cohesive model named as adaptive cohesive model (ACM), for stably and accurately simulating delamination propagations in composite laminates under transverse loads. In this model, a pre-softening zone is proposed ahead of the existing softening zone. In this pre-softening zone, with the increase of effective relative displacements at the integration points of cohesive elements on interfaces, the initial stiffnesses and interface strengths at these points are reduced gradually. However, the onset displacement for starting the real softening process is not changed in this model. The critical energy release rate or fracture toughness of materials for determining the final displacement of complete decohesion is kept constant. Also, the traction based model includes a cohesive zone viscosity parameter (η) to vary the degree of rate dependence and to adjust the peak or maximum traction.

In this Chapter, this cohesive model is formulated and implemented in LS-DYNA (Livermore Software Technology Corporation, 2005) as a user defined materials (UMAT). LS-DYNA is one of the explicit FE codes most widely used by the automobile and aerospace industries. It has a large library of material options; however, continuous cohesive elements are not available within the code. The formulation of this model is fully three dimensional and can simulate mixed-mode delamination. However, the objective of this study is to develop new adaptive cohesive elements able to capture delamination onset and growth under quasi-static and dynamic Mode-I loading conditions. The capabilities of the proposed elements are proven by comparing the numerical simulations and the experimental results of DCB in Mode-I.

2. The constitutive model

Cohesive elements are used to model the interface between sublaminates. The element consists of a near zero-thickness volumetric element in which the interpolation shape functions for the top and bottom faces are compatible with the kinematics of the elements that are being connected to it (Davila et al., 2001). Cohesive elements are typically formulated in terms of traction vs. relative displacement relationship. In order to predict the initiation and growth of delamination, an 8-node cohesive element shown in figure 1 is developed to overcome the numerical instabilities.

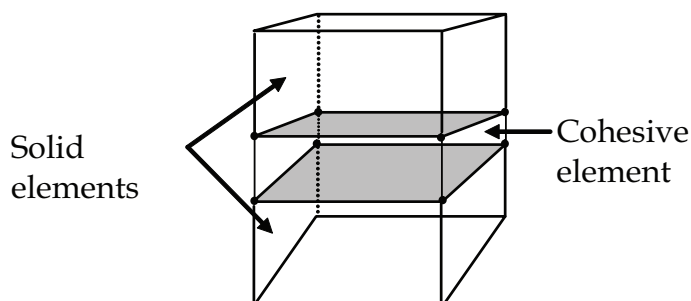


Fig. 1. Eight-node cohesive element

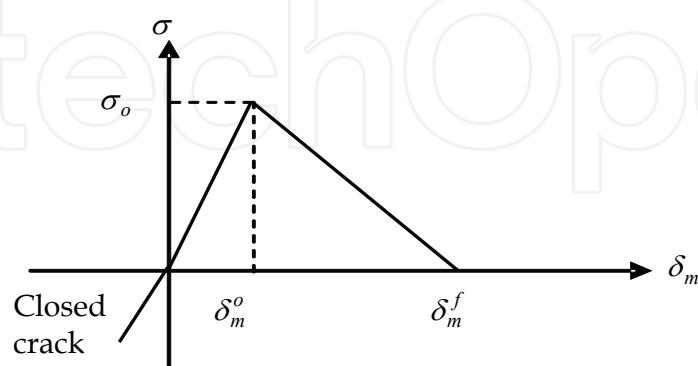


Fig. 2. Normal (bilinear) constitutive model

The need for an appropriate constitutive equation in the formulation of the interface element is fundamental for an accurate simulation of the interlaminar cracking process. A constitutive equation is used to relate the traction to the relative displacement at the

interface. The bilinear model, as shown in figure 2, is the simplest model to be used among many strain softening models. Moreover, it has been successfully used by several authors in implicit analyses (De Moura et al., 2000; Camanho et al., 2003; Pinho et al., 2004; Pinho et al., 2006).

However, using the bilinear model leads to numerical instabilities in an explicit implementation. To overcome this numerical instability, a new adaptive model is proposed by Hu et al. (Hu et al., 2008) and presented in this Chapter as shown in figure 3. The adaptive interfacial constitutive response shown in figure 3 is implemented as follows:

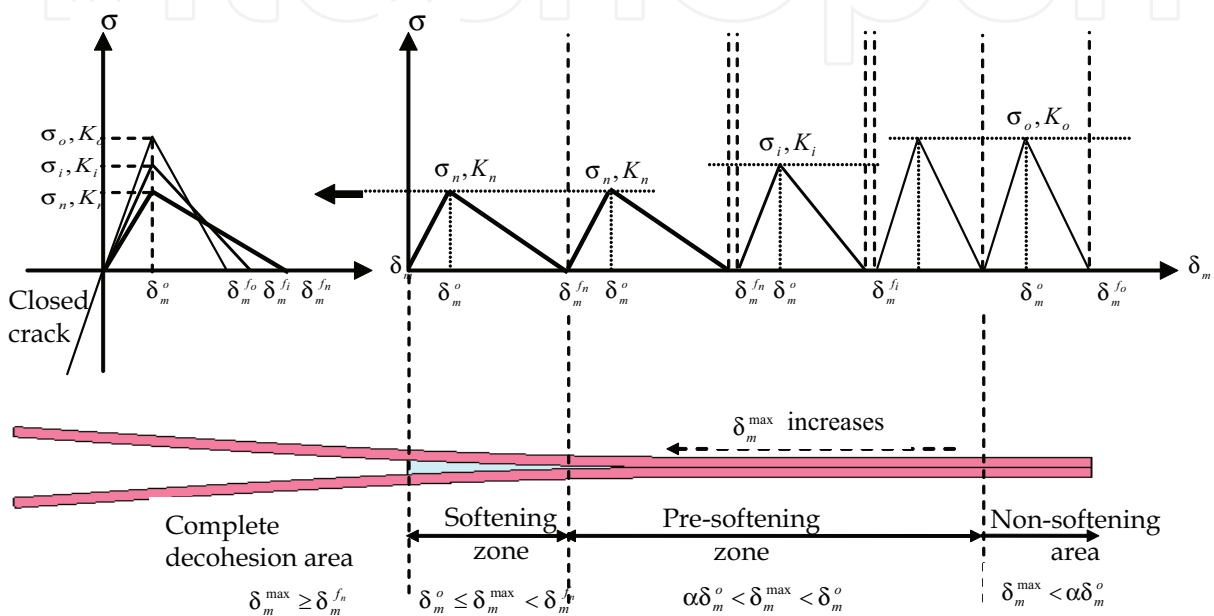


Fig. 3. Adaptive constitutive model for Mode-I (Hu et.al, 2008)

In pre-softening zone, $\alpha\delta_m^o < \delta_m^{\max} < \delta_m^o$, the constitutive equation is given by

$$\sigma = (\sigma_m + \eta\dot{\delta}_m) \frac{\delta_m}{\delta_m^o} \tag{1}$$

and

$$\sigma_m = K\delta_m^o \tag{2}$$

where σ is the traction, K is the penalty stiffness and can be written as

$$K = \begin{cases} K_o & \delta_m \leq 0 \\ K_i & \delta_m^{\max} < \delta_m^o \\ K_n & \delta_m^o \leq \delta_m^{\max} < \delta_m^f \end{cases} \tag{3}$$

δ_m is the relative displacement in the interface between the top and bottom surfaces (in this study, it equals the normal relative displacement for Mode-I), δ_m^o is the onset displacement and it is remained constant in the simulation and can be determined as follows:

$$\delta_m^o = \frac{\sigma_o}{K_o} = \frac{\sigma_i}{K_i} = \frac{\sigma_{\min}}{K_{\min}} \quad (4)$$

where σ_o is the initial interface strength, σ_i is the updated interface strength in the pre-softening zone, σ_{\min} is the minimum limit of the interface strength, K_o is the initial stiffness, K_i is the updated stiffness in the pre-softening zone, and K_{\min} is the minimum value of the stiffness. For each increment and for time $t+1$, δ_m is updated as follows:

$$\delta_m^{t+1} = t_c \varepsilon^{t+1} - t_c \quad (5)$$

where t_c is the thickness of the cohesive element and ε^{t+1} is the normal strain of the cohesive element for time $t+1$, $\varepsilon^{t+1} = \varepsilon^t + \Delta\varepsilon$, where $\Delta\varepsilon$ is the normal strain increment. The $(\delta_m^{\max})^t$ is the max relative displacement of the cohesive element occurs in the deformation history. For each increment and for time $t+1$, δ_m^{\max} is updated as follows:

$$(\delta_m^{\max})^{t+1} = \delta_m^{t+1} \quad \text{if } \delta_m^{t+1} \geq (\delta_m^{\max})^t \quad \text{and,} \quad (6)$$

$$(\delta_m^{\max})^{t+1} = (\delta_m^{\max})^t \quad \text{if } \delta_m^{t+1} < (\delta_m^{\max})^t \quad (7)$$

Using the max value of the relative displacement δ_m^{\max} rather than the current value δ_m prevents healing of the interface. The updated stiffness and interface strength are determined in the following forms:

$$\sigma_i = \frac{\delta_m^{\max}}{\delta_m^o} (\sigma_{\min} - \sigma_o) + \sigma_o, \quad \sigma_o > \sigma_{\min} \quad \text{and} \quad (\alpha \delta_m^o < \delta_m^{\max} < \delta_m^o) \quad (8)$$

$$K_i = \frac{\delta_m^{\max}}{\delta_m^o} (K_{\min} - K_o) + K_o, \quad K_o > K_{\min} \quad \text{and} \quad (\alpha \delta_m^o < \delta_m^{\max} < \delta_m^o) \quad (9)$$

It should be noted that α in equations (8) and (9) is a parameter to define the size of pre-softening zone. When $\alpha = 1$, the present adaptive cohesive mode degenerates into the traditional cohesive model. In these computations, α was set to zero. From our numerical experiences, the size of pre-softening zone has some influences on the initial stiffness of loading-displacement curves, but not so significant. The reason is that for the region far always from the crack tip, the interface decrease or update according to equations (8) and (9) is not obvious since δ_m^{\max} is very small. The energy release rate for Mode-I G_{IC} also remains constant. Therefore, the final displacements associated to the complete decohesion δ_m^{fi} are adjusted as shown in figure 3 as

$$\delta_m^{fi} = \frac{2G_{IC}}{\sigma_i} \quad (10)$$

Once the max relative displacement of an element located at the crack front satisfies the following conditions; $\delta_m^{\max} > \delta_m^o$, this element enters into the real softening process. Where, as shown in figure 3, the real softening process denotes a stiffness decreasing process caused by accumulated damages. Then, the current strength σ_n and stiffness K_n , which are almost equal to σ_{\min} and K_{\min} , respectively, will be used in the softening zone.

2. In softening zone, $\delta_m^o \leq \delta_m^{\max} < \delta_m^f$, the constitutive equation is given by

$$\sigma = (1 - d)(\sigma_m + \eta \dot{\delta}_m) \frac{\delta_m}{\delta_m^o} \quad (11)$$

where d is the damage variable and can be defined as

$$d = \frac{\delta_m^f (\delta_m^{\max} - \delta_m^o)}{\delta_m^{\max} (\delta_m^f - \delta_m^o)}, \quad d \in [0, 1] \quad (12)$$

The above adaptive cohesive mode is of the engineering meaning when using coarse meshes for complex composite structures, which is, in fact, an 'artificial' means for achieving the stable numerical simulation process. A reasonable explanation is that all numerical techniques are artificial, whose accuracy strongly depends on their mesh sizes, especially at the front of crack tip. To remove the factitious errors in the simulation results caused by the coarse mesh sizes in the numerical techniques, some material properties are artificially adjusted in order to partially alleviate or remove the numerical errors. Otherwise, very fine meshes need to be used, which may be computationally impractical for very complex problems from the capabilities of most current computers. Of course, the modified material parameters should be those which do not have the dominant influences on the physical phenomena. For example, the interface strength usually controls the initiation of interface cracks. However, it is not crucial for determining the crack propagation process and final crack size from the viewpoint of fracture mechanics. Moreover, there has been almost no clear rule to exactly determine the interface stiffness, which is a parameter determined with a high degree of freedom in practical cases. Therefore, the effect of the modifications of interface strength and stiffness can be very small since the practically used onset displacement δ_m^o for delamination initiation is remained constant in our model. For the parameters, which dominate the fracture phenomena, should be unchanged. For instance, in our model, the fracture toughness dominating the behaviors of interface damages is kept constant.

3. Information finite element implementation

The proposed cohesive element is implemented in LS-DYNA finite element code as a user defined material (UMAT) using the standard library 8-node solid brick element and *MAT_USER_DEFINED_MATERIAL_MODELS. The keyword input has to be used for the user interface with data. The following cards are used (LSDYNA User's Manual; LSTC, 2005) as shown in table 1.

This approach for the implementation requires modelling the resin rich layer as a non-zero thickness medium. In fact, this layer has a finite thickness and the volume associated with the cohesive element can in fact set to be very small by using a very small thickness (e.g. 0.01 mm). To verify these procedures, the crack growth along the interface of a double cantilever beam (DCB) is studied. The two arms are modelled using standard LS-DYNA 8-node solid brick elements and the interface elements are developed in a FORTRAN subroutine using the algorithm shown in figure 4.

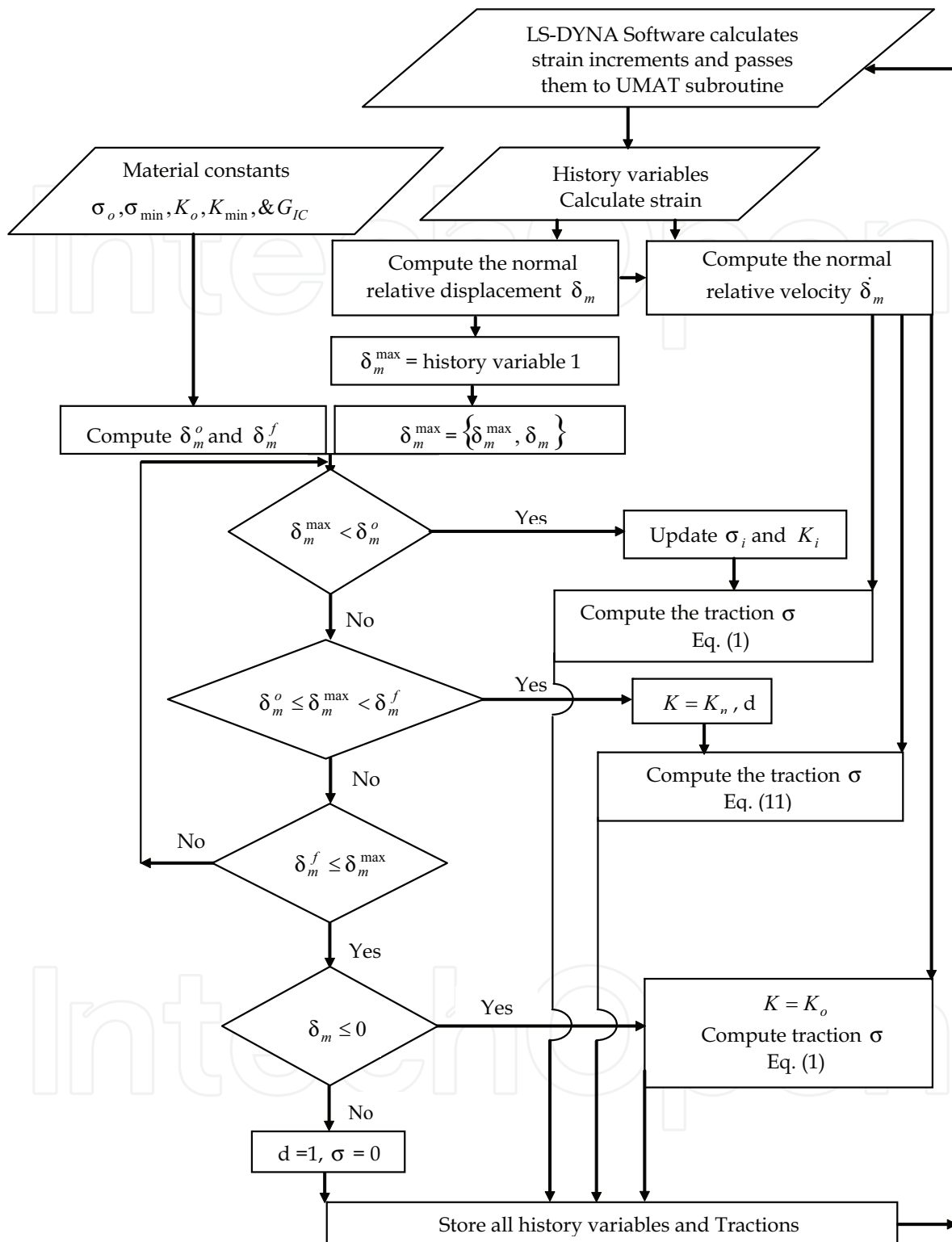


Fig. 4. Flow chart for traction computation in Mode-I

The LS-DYNA code calculates the strain increments for a time step and passes them to the UMAT subroutine at the beginning of each time step. The material constants, such as the stiffness and strength, are read from the LS-DYNA input file by the subroutine. The current and maximum relative displacements are saved as history variables which can be read in by

the subroutine. Using the history variables, material constants, and strain increments, the subroutine is able to calculate the stresses at the end of the time step by using the constitutive equations. The subroutine then updates and saves the history variables for use in the next time step and outputs the calculated stresses. Note that the *DATABASE _ EXTENT _ BINARY command is required to specify the storage of history variables in the output file.

Variable	MID	RO	MT	LMC	NHV	IORTHO	IBULK	IG
Type	I	F	I	I	I	I	I	I
Variable	IVECT	IFAIL	ITHERM	IHYPER	IEOS			
Type	I	I	I	I	I			
Variable	AOPT	MAXC	XP	YP	ZP	A1	A2	A3
Type	F	F	F	F	F	F	F	F
Variable	V1	V2	V3	D1	D2	D3	BETA	
Type	F	F	F	F	F	F	F	
Variable	P1	P2	P3	P4	P5	P6	P7	P8
Type	F	F	F	F	F	F	F	F

where

MID: Material identification; RO: Mass density; MT: User material type (41-50 inclusive); LMC: Length of material constant array which is equal to the number of material constant to be input; NHV: Number of history variables to be stored; IORTHO: Set to 1 if the material is orthotropic; IBULK: Address of bulk modulus in material constants array; IG: Address of shear modulus in material constants array; IVECT: Vectorization flag (on=1), a vectorized user subroutine must be supplied; IFAIL: Failure flag (on=1, allows failure of shell elements due to a material failure criterion; ITHERM: Temperature flag (on=1), compute element temperature; AOPT: Material axes option; MAXC: Material axes change flag for brick elements; XP,YP,ZP: Coordinates of point p for AOPT=1; A1,A2,A3: Components of vector a AOPT=2; V1,V2,V3: Components of vector v AOPT=3; D1,D2,D3: Components of vector d AOPT=2; BETA: Material angle in degrees for AOPT=3; P1..P8.: Material parameter (LSDYNA User's Manual; LSTC, 2005).

Table 1. Keyword cards for UMAT (LSDYNA User's Manual; LSTC, 2005)

It is worth noting that the stable explicit time step is inversely proportional to the maximum natural frequency in the analysis. The small thickness elements drive up the highest natural frequency, therefore, it drives down the stable time step. Hence, mass scaling is used to obtain faster solutions by achieving a larger explicit time step when applying the cohesive element to quasi-static situations. Note that the volume associated with the cohesive element would be small by using a small thickness and the element's kinetic energy arising from this be still several orders of magnitude below its internal energy, which is an important consideration for quasi-static analyses to minimize the inertial effects.

4. Numerical simulations

4.1 Quasi-static analysis

The DCB specimen is made of a unidirectional fibre-reinforced laminate containing a thin insert at the mid-plane near the loaded end. A 150 mm long specimen (L), 20 mm wide (w)

and composed of two thick plies of unidirectional material ($2h = 2 \times 1.98$ mm) shown in figure 5 was tested by Morais (Morais et al., 2000). The initial crack length (l_c) is 55 mm. A displacement rate of 10 mm/sec is applied to the appropriate points of the model. The properties of both carbon fiber-reinforced epoxy material and the interface are given in table 2.

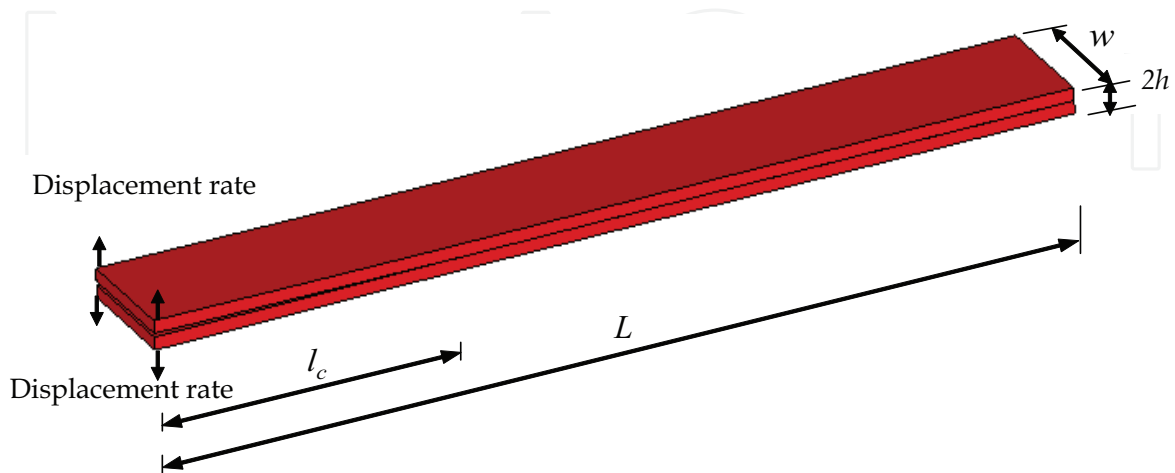


Fig. 5. Model of DCB specimen

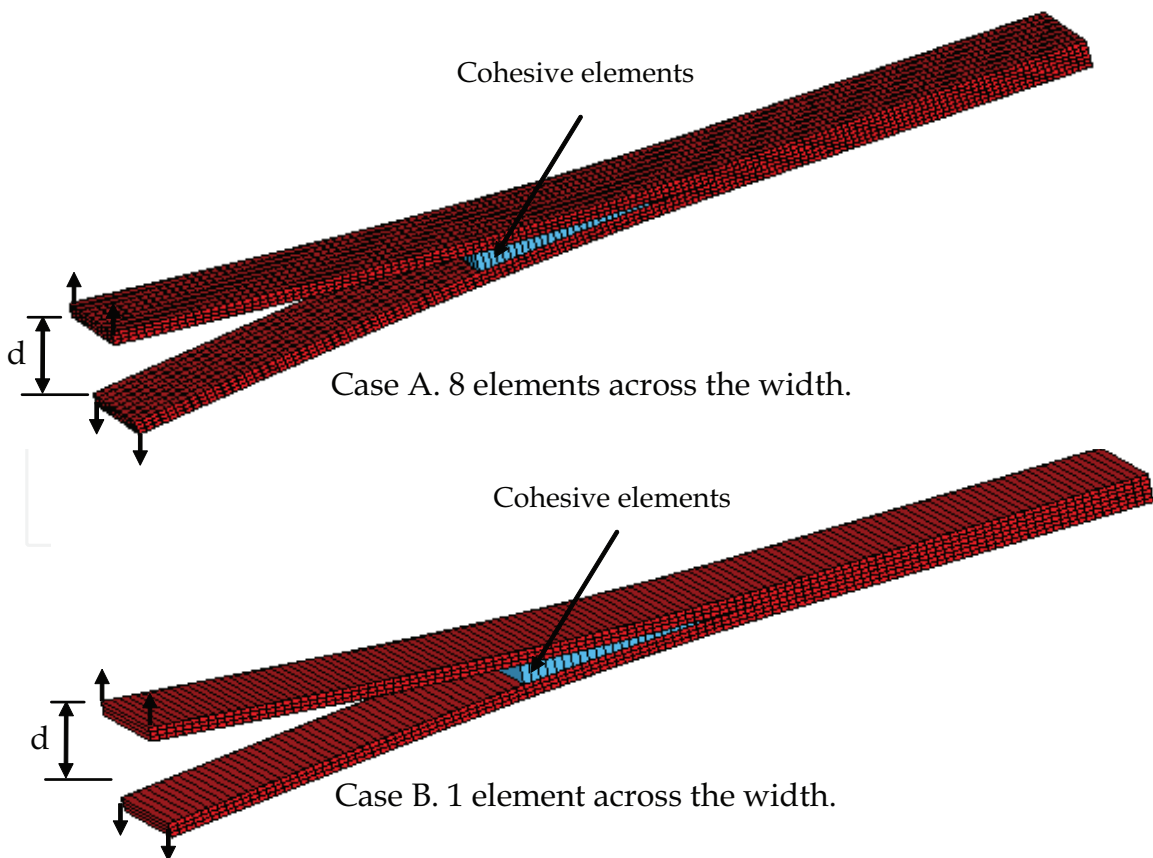


Fig. 6. LS-DYNA finite element model of the deformed DCB specimen

Carbon fiber- reinforced epoxy material	DCB specimen interface
$\rho = 1444 \text{ kg/m}^3$	$G_{IC} = 0.378 \text{ kJ/m}^2$
$E_{11} = 150 \text{ GPa}, E_{22} = E_{33} = 11 \text{ GPa}$	$K_o = 3 \times 10^4 \text{ N/mm}^3$
$\nu_{12} = \nu_{13} = 0.25, \nu_{23} = 0.45$	$\sigma_o = 45 \text{ MPa}$ case I
$G_{12} = G_{13} = 6.0 \text{ MPa}, G_{23} = 3.7 \text{ MPa}$	$\sigma_o = 60 \text{ MPa}$ case II

Table 2. Properties of both carbon fiber-reinforced epoxy material and specimen interface

The LS-DYNA finite element model, which is shown deformed in figure 6, consists of two layers of fully integrated S/R 8-noded solid elements, with 3 elements across the thickness. Two cases with different mesh sizes are used in the initial analysis, namely: case A, which includes eight elements across the width, and case B, which includes one element across the width, respectively. The two cases are compared using the new cohesive elements with mesh size of 1 mm to figure out the anticlastic effects.

A plot of a reaction force as a function of the applied end displacement is shown in figure 7. It is clearly shown that both cases bring similar results with peak load value of 64 N. Therefore, the anticlastic effects are neglected and only one element (case B) is used across the width in the following analyses.

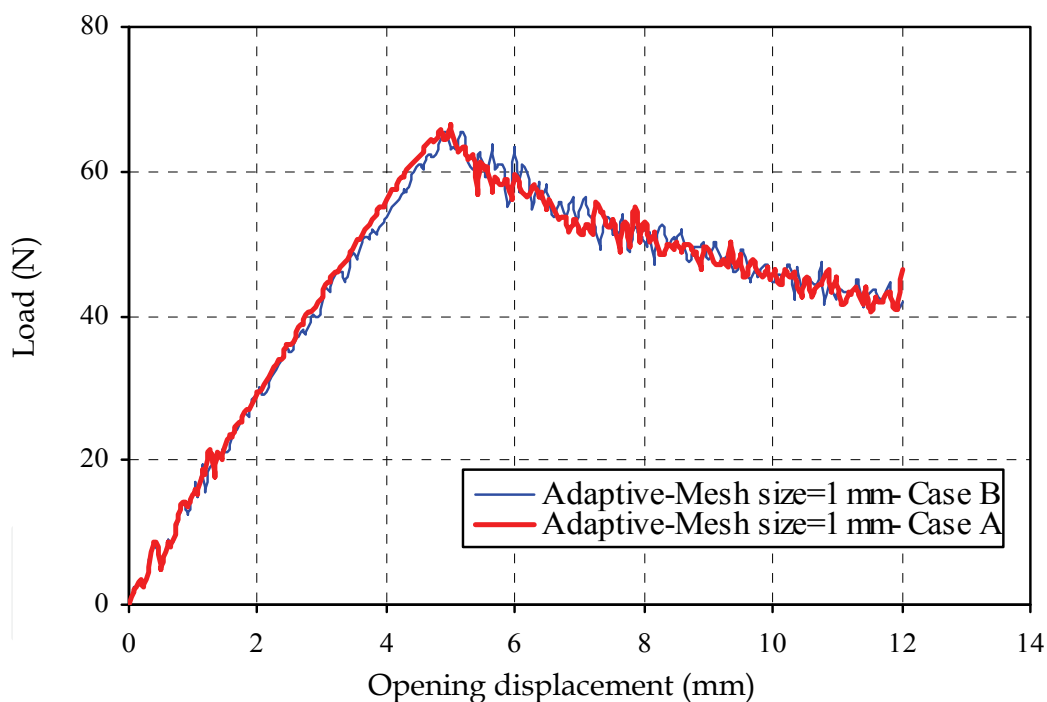


Fig. 7. Load-displacement curves for a DCB specimen in both cases A and B

Different cases are considered in this study and given in table 3 to investigate the influence of the new adaptive cohesive element using different mesh sizes. The aim of the first five cases is to study the effect of the element size with constant values of interface strength and stiffness on the load-displacement relationship. Different element sizes are used along the interface spanning from very small size of 0.5 mm to coarse mesh of 2 mm. Moreover, cases 3, 6, and 7 are to study the effect of the value of minimum interface strength on the results. Finally, Cases 6 and 8 are to find out the effect of the high interfacial strength.

Case 1	Mesh size = 2 mm	$\sigma_o = 45 \text{ MPa}$, $\sigma_{\min} = 15 \text{ Mpa}$	$K_o = 3 \times 10^4 \text{ N/mm}^3$, $K_{\min} = 1 \times 10^4 \text{ N/mm}^3$
Case 2	Mesh size = 1.25 mm	$\sigma_o = 45 \text{ MPa}$, $\sigma_{\min} = 15 \text{ Mpa}$	$K_o = 3 \times 10^4 \text{ N/mm}^3$, $K_{\min} = 1 \times 10^4 \text{ N/mm}^3$
Case 3	Mesh size = 1 mm	$\sigma_o = 45 \text{ MPa}$, $\sigma_{\min} = 15 \text{ Mpa}$	$K_o = 3 \times 10^4 \text{ N/mm}^3$, $K_{\min} = 1 \times 10^4 \text{ N/mm}^3$
Case 4	Mesh size = 0.75 mm	$\sigma_o = 45 \text{ MPa}$, $\sigma_{\min} = 15 \text{ Mpa}$	$K_o = 3 \times 10^4 \text{ N/mm}^3$, $K_{\min} = 1 \times 10^4 \text{ N/mm}^3$
Case 5	Mesh size = 0.5 mm	$\sigma_o = 45 \text{ MPa}$, $\sigma_{\min} = 15 \text{ MPa}$	$K_o = 3 \times 10^4 \text{ N/mm}^3$, $K_{\min} = 1 \times 10^4 \text{ N/mm}^3$
Case 6	Mesh size = 1 mm	$\sigma_o = 45 \text{ MPa}$, $\sigma_{\min} = 22.5 \text{ MPa}$	$K_o = 3 \times 10^4 \text{ N/mm}^3$, $K_{\min} = 1.5 \times 10^4 \text{ N/mm}^3$
Case 7	Mesh size = 1 mm	$\sigma_o = 45 \text{ MPa}$, $\sigma_{\min} = 10 \text{ MPa}$	$K_o = 3 \times 10^4 \text{ N/mm}^3$, $K_{\min} = 0.667 \times 10^4 \text{ N/mm}^3$
Case 8	Mesh size = 1 mm	$\sigma_o = 60 \text{ MPa}$, $\sigma_{\min} = 30 \text{ MPa}$	$K_o = 3 \times 10^4 \text{ N/mm}^3$, $K_{\min} = 1.5 \times 10^4 \text{ N/mm}^3$

Table 3. Different cases of analyses

Figures 8 and 9 show the load-displacement curves for both normal (bilinear) and adaptive cohesive elements in cases 1 and 5, respectively, with different element sizes.

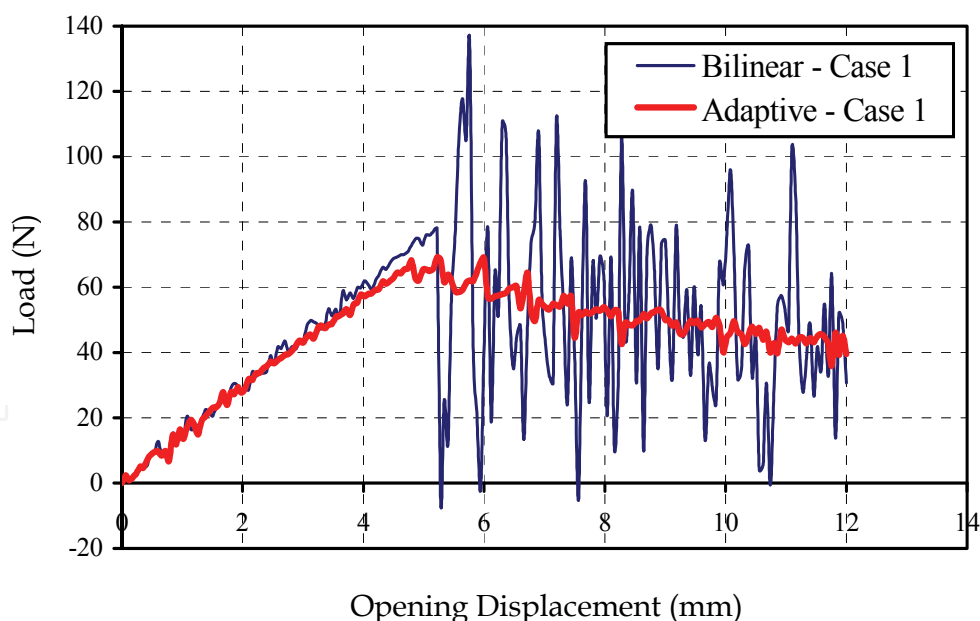


Fig. 8. Load-displacement curves obtained using both bilinear and adaptive formulations- case 1

Figure 8 clearly shows that the bilinear formulation results in a severe instability once the crack starts propagating. However, the adaptive constitutive law is able to model the

smooth, progressive crack propagation. It is worth mentioning that the bilinear formulation brings smooth results by decreasing the element size. And it is clearly noticeable from figure 9 that both bilinear and adaptive formulations are found to be stable in case 5 with very small element size. This indicates that elements with very small sizes need to be used in the softening zone to obtain high accuracy using bilinear formulation. However, this leads to large computational costs compare to case 1. On the other hand, figure 10, which presents the load-displacement curves, obtained with the use of the adaptive formulation in the first five cases, show a great agreement of the results regardless the mesh size. Adaptive cohesive model (ACM) can yield very good results from the aspects of the peak load and the slope of loading curve if σ_{\min} is properly defined. From this figure, it can be found that the different mesh sizes result in almost the same loading curves. Even, with 2 mm mesh size, which considerable large size, although the oscillation is higher compared with those of fine mesh size, ACM still models the propagation in stable manner. The oscillation of the curve once the crack starts propagates became less by decreasing the mesh size. Therefore, the new adaptive model can be used with considerably larger mesh size and the computational cost will be greatly minimized.

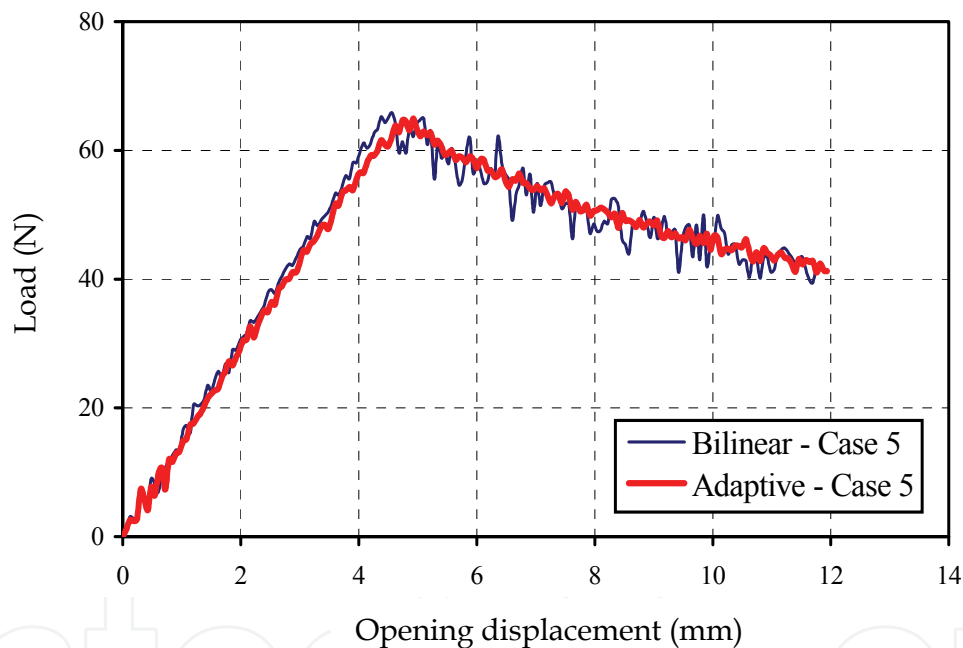


Fig. 9. Load-displacement curves obtained using both bilinear and adaptive formulations- case 5

The load-displacement curves obtained from the numerical simulation of cases 3, 6 and 7 are presented in figure 11 together with experimental data (Camanho & Davila, 2002). It can be seen that the average maximum load obtained in the experiments is 62.5 N, whereas the average maximum load predicted from the three cases is 65 N. It can be observed that numerical curves slightly overestimate the load. It is worth noting that with the decrease of interface strength, the result is stable, very good result can be obtained by comparing with the experimental ones, however, the slope of loading curve before the peak load is obviously lower than those of experimental ones (case 7; $\sigma_{\min}=10.0$ MPa). In case 6 ($\sigma_{\min}=22.5$ MPa) and case 3 ($\sigma_{\min}=15$ MPa), excellent agreements between the experimental data and the

numerical predictions is obtained although the oscillation in case 6 is higher compared with those of case 3. Also, the slope of loading curve in case 3 is closer to the experimental results compared with that in case 6.

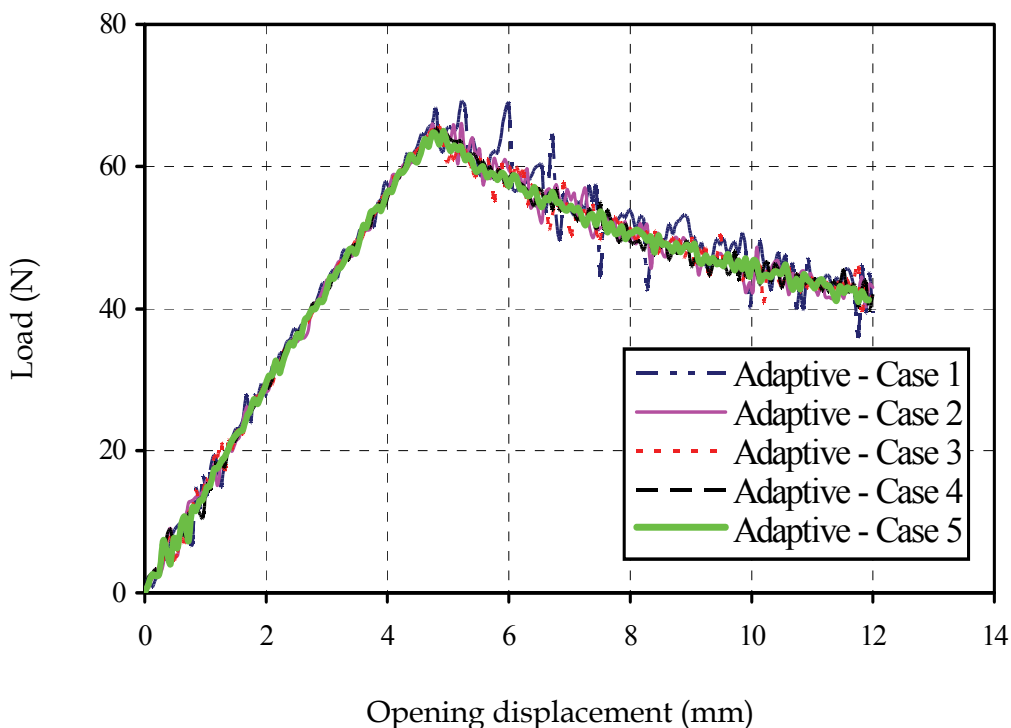


Fig. 10. Load-displacement curves obtained using the adaptive formulation-cases 1-5

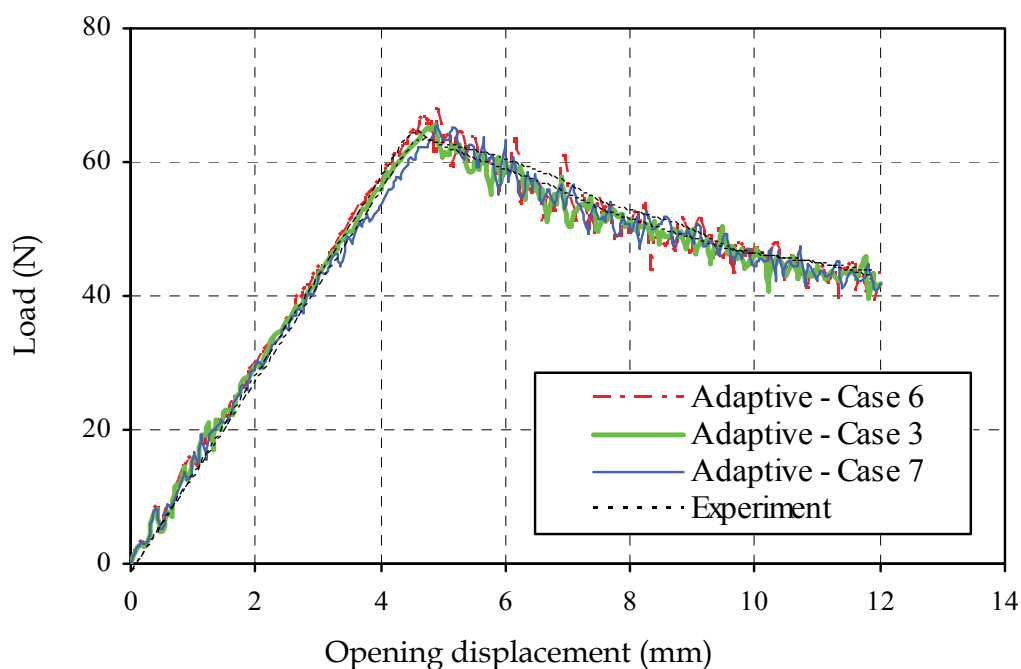


Fig. 11. Comparison of experimental and numerical simulations using the adaptive formulation - cases 3, 6 and 7

Figure 12 show the load-displacement curves of the numerical simulations obtained using the bilinear formulation in both cases, i.e., cases 6 and 8.

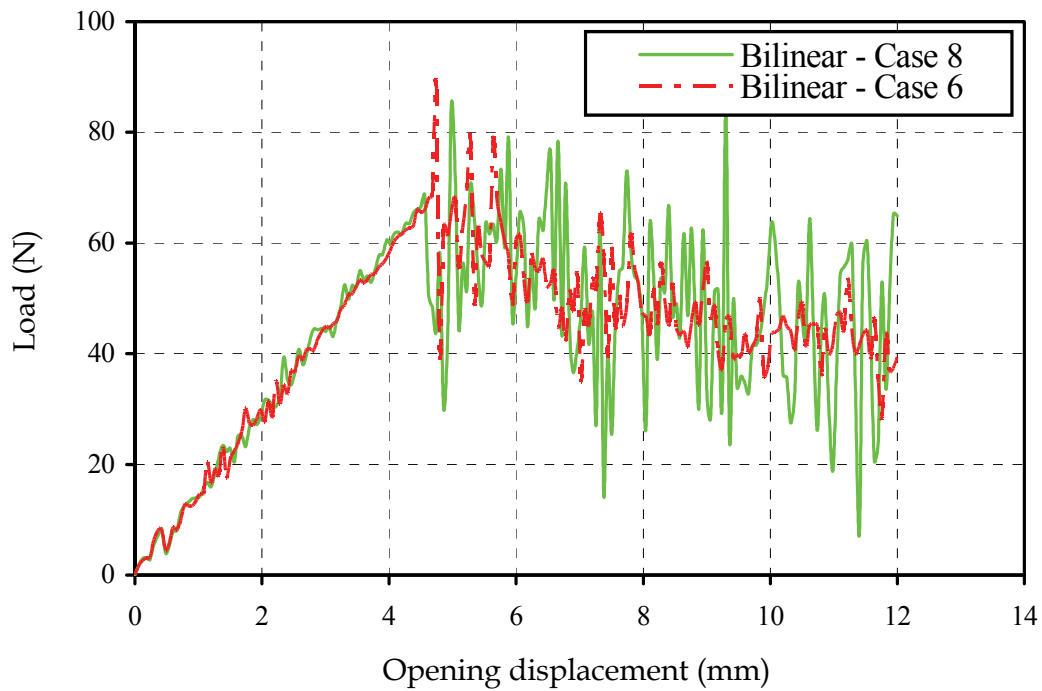


Fig. 12. Load-displacement curves obtained using the bilinear formulation- cases 6 and 8

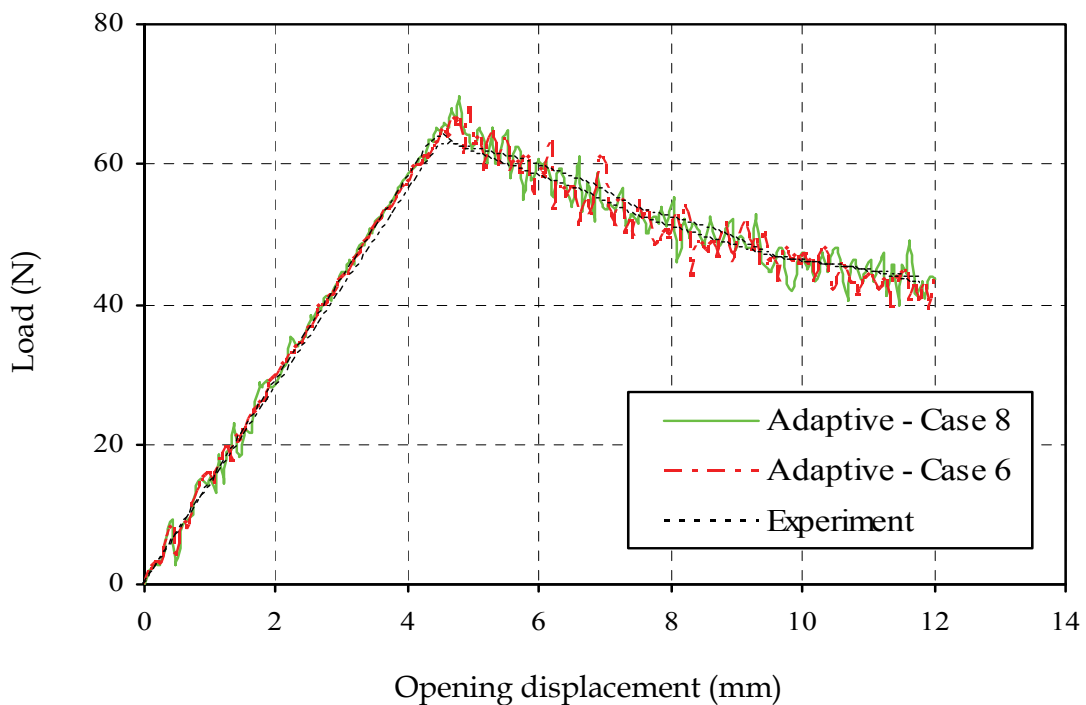


Fig. 13. Comparison of experimental and numerical simulations using the adaptive formulation-cases 6 and 8

The bilinear formulations results in a severe instabilities once the crack starts propagation. It is also shown that a higher maximum traction (case 8) resulted in a more severe instability compared to a lower maximum traction (case 6). However, as shown in figure 13, the load-displacement curves of the numerical simulations obtained using the adaptive formulations are very similar in both cases. The maximum load obtained from case 8 is found to be 69 N while in case 6, the maximum load obtained is 66 N. The adaptive formulation is able to model the smooth, progressive crack propagation and also to produce close results compared with the experimental ones.

4.2 Dynamic analysis

The DCB specimen, as shown in figure 5, is made of an isotropic fibre-reinforced laminate containing a thin insert at the mid-plane near the loaded end, $L=250$ mm, $w=25$ mm and $h=1.5$ mm, was analyzed by Moshier (Moshier, 2006). The initial crack length (l_c) is 34 mm. A displacement rate of 650 mm/sec is applied to the appropriate points of the model. Young's modulus, density and Poisson's ratio of carbon fibre-reinforced epoxy material are given as $E=115$ GPa, $\rho=1566$ Kg/m³, and $\nu=0.27$, respectively. The properties of the DCB specimen interface are given as following: $G_{IC}=0.7$ kJ/m², $K_o=1 \times 10^5$ N/mm³, $K_{min}=0.333 \times 10^5$ N/mm³, $\sigma_o=50$ MPa, and $\sigma_{min}=16.67$ MPa

Similarly, the LS-DYNA finite element model consists of two layers of fully integrated S/R 8-noded solid elements, with 3 elements across the thickness. The adaptive rate-dependent cohesive zone model is implemented using a user defined cohesive material model in LS-DYNA. Two different values of viscosity parameter are used in the simulations; $\eta=0.01$ and 1.0 N·sec/mm³, respectively. Note that η is a material parameter depending on deformation rate, which appears in equations (1) and (11). When $\eta=0$, it would be a traditional model without rate dependence. By observing equation (1), η determines the ratio between viscosity stress $\eta\dot{\delta}_m$ and interface strength σ_m since $\sigma_m=\sigma_i$ if equations (1) and (4) are considered by setting $K=K_i$. For example, if $\dot{\delta}_m=6.5$ mm/sec is assumed on the interface here (i.e. 1% of loading rate). $\eta=0.01$ N·sec/mm³ corresponds to a low viscosity stress of 0.065MPa, which is much lower than the initial interface strength of 50 MPa. However, $\eta=1.0$ N·sec/mm³ corresponds to a viscosity stress of 6.5 MPa, which is around 13% of the interface strength, and denotes a higher rate dependence. In addition, two sets of simulations are performed here. The first set involves simulations of normal (bilinear) cohesive model. The second set involves simulations of the new adaptive rate-dependent model.

A plot of a reaction force as a function of the applied end displacement of the DCB specimen using cohesive elements with viscosity value of 0.01 N·sec/mm³ is shown in figure 14. It is clearly shown from figure 14 that the bilinear formulation results in a severe instability once the crack starts propagating. However, the adaptive constitutive law is able to model the smooth, progressive crack propagation. It is worth mentioning that the bilinear formulation might bring smooth results by decreasing the element size.

The load-displacement curves obtained from the numerical simulation of both bilinear and adaptive cohesive model using viscosity parameter of 1.0 N·sec/mm³ is presented in figure 15. It can be seen that, again, the adaptive constitutive law is able to model the smooth, progressive crack propagation while the bilinear formulation results in a severe instability once the crack starts propagating. The average maximum load obtained using the adaptive

rate dependent model is 110 N, whereas the average maximum load predicted from the bilinear model is 120 N.

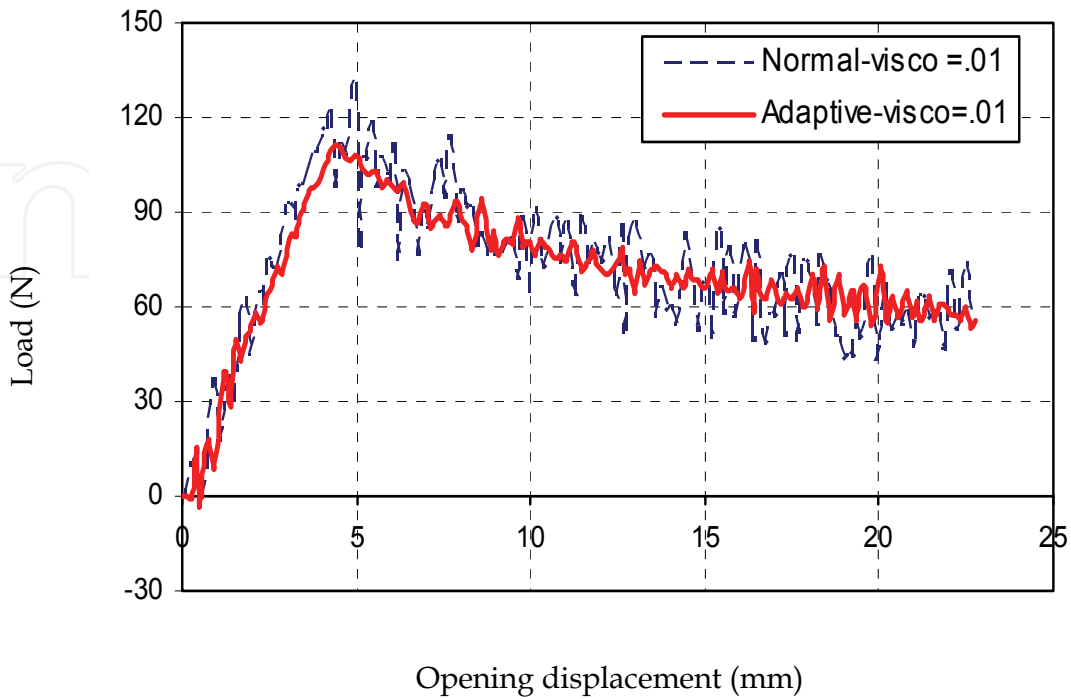


Fig. 14. Load-displacement curves obtained using both bilinear and adaptive formulations ($\eta = 0.01$)

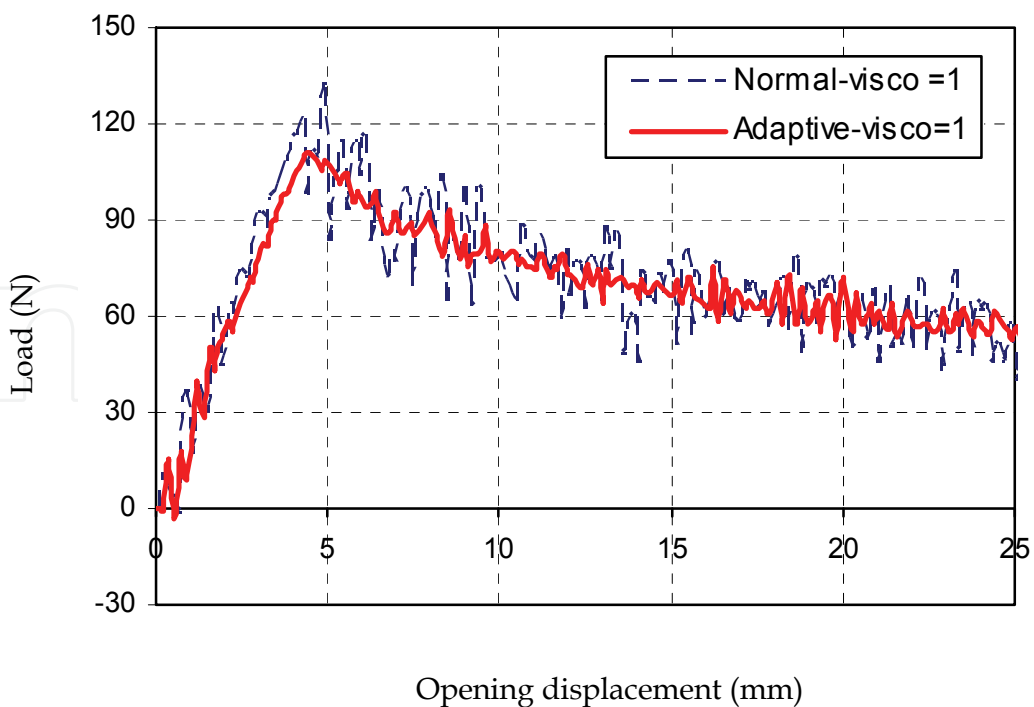


Fig. 15. Load-displacement curves obtained using both bilinear and adaptive formulations ($\eta = 1$)

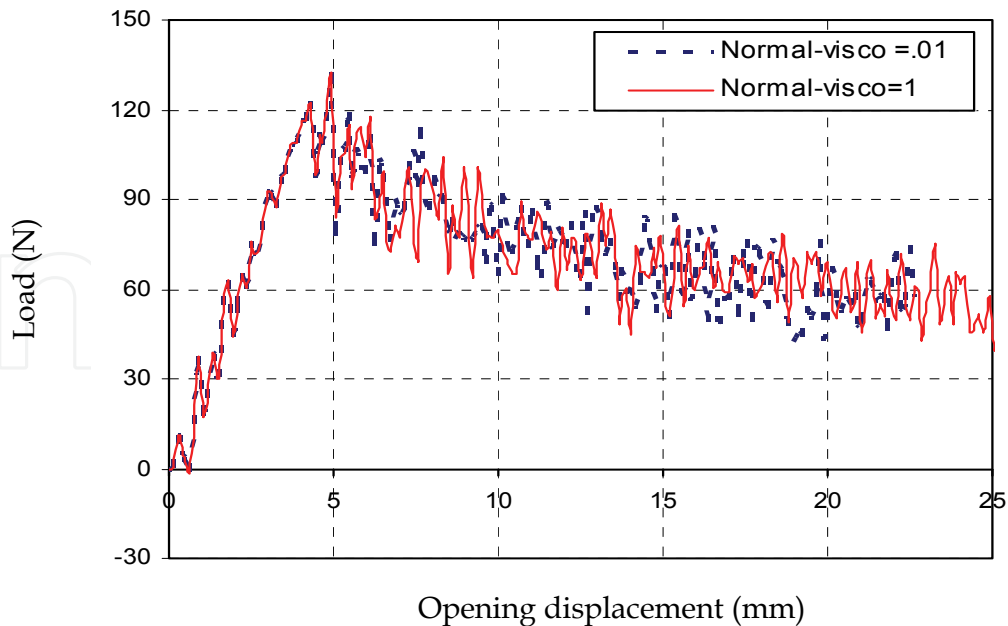


Fig. 16. Load-displacement curves obtained using bilinear formulations ($\eta = 0.01,1$)

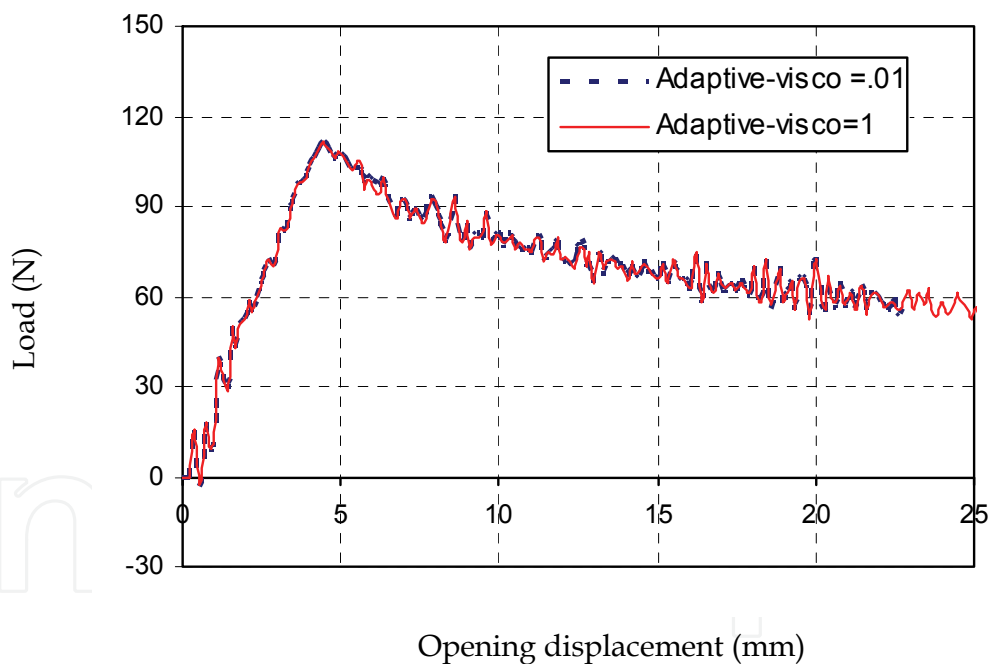


Fig. 17. Load-displacement curves obtained using adaptive formulations ($\eta = 0.01,1$)

Figure 16 shows the load-displacement curves of the numerical simulations obtained using the bilinear formulation with two different viscosity parameters, 0.01 and 1.0 N·sec/mm³, respectively. It is noticed from figure 16 that, in both cases, the bilinear formulation results in severe instabilities once the crack starts propagation. There is a very slight improvement to model the smooth, progressive crack propagation using bilinear formulations with a high viscosity parameter. On the other hand, the load-displacement curves of the numerical simulations obtained using the new adaptive formulation with two different viscosity

parameters, 0.01 and 1.0 N·sec/mm³, respectively, is depicted in figure 17. It is clear from figure 17 that the adaptive formulation is able to model the smooth, progressive crack propagation irrespective of the value of the viscosity parameter. More parametric studies will be performed in the ongoing research to accurately predict the effect of very high values of viscosity parameter on the results using both bilinear and adaptive cohesive element formulations.

5. Conclusions

A new adaptive cohesive element is developed and implemented in LS-DYNA to overcome the numerical instability occurred using the bilinear cohesive model. The formulation is fully three dimensional, and can be simulating mixed-mode delamination, however, in this study, only DCB test in Mode-I is used as a reference to validate the numerical simulations. Quasi-static and dynamic analyses are carried out in this research to study the effect of the new constitutive model. Numerical simulations showed that the new model is able to model the smooth, progressive crack propagation. Furthermore, the new model can be effectively used in a range of different element sizes (reasonably coarse mesh) and can save a large amount of computation. The capability of the new model is proved by the great agreement obtained between the numerical simulations and the experimental results.

6. Acknowledgement

The author wishes to acknowledge the research support and constitutive models provided for this ongoing research by Professor Ning Hu.

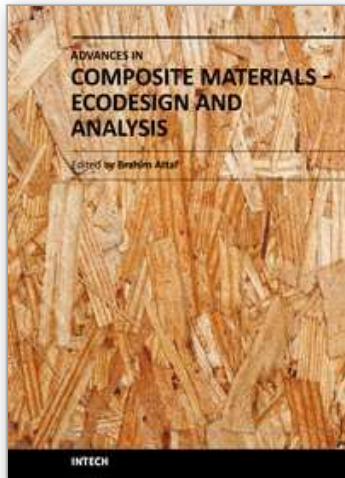
7. References

- Camanho, P. & Davila, C. (2004). Fracture analysis of composite co-cured structural joints using decohesion elements. *Journal of Fatigue & Fracture of Engineering Materials & Structures*, Vol. 27, 745-757
- Camanho, P.; Davila, C. & De Moura, M. (2003). Numerical simulation of mixed-mode progressive delamination in composite materials. *Journal of Composite Materials*, Vol. 37, No. 16, 1415-38
- Camanho, P. & Davila C. (2002). Mixed-mode decohesion finite elements for the simulation of delamination in composite materials. NASA/TM-2002-211737, 1-37
- Camanho, P.; Davila, C. & Ambur, D. (2001). Numerical simulation of delamination growth in composite materials. NASA-TP-211041, 1-19
- Chen, J.; Crisfield, M.; Kinloch, A.; Busso, E.; Matthews, F. & Qiu, Y. (1999). Predicting progressive delamination of composite material specimens via interface elements. *Mechanics of Composite Material and Structures*, Vol. 6, No. 4, 301-317
- Costanzo, F. & Walton, J. (1997). A study of dynamic crack growth in elastic materials using a cohesive zone model. *International Journal of Engineering Science*, Vol. 35, No. 12/13, 1085-1114
- Cui, W. & Wisnom, M. (1993). A combined stress-based and fracture mechanics-based model for predicting delamination in composites. *Composites*, Vol. 24, 467-474

- Davila, C.; Camanho, P. & De Moura M. (2001). Mixed-mode decohesion elements for analyses of progressive delamination. *42nd AIAA/ASME/ASCE/AHS/ASC Structures, Structural Dynamics and Material Conference*, pp. 1-12, April 2001, Washington, USA
- De Moura, M.; Gonçalves, J.; Marques, A. & De Castro, P. (2000). Prediction of compressive strength of carbon-epoxy laminates containing delaminations by using a mixed-mode damage model. *Composite Structure*, Vol. 50, No. 2, 151-157
- De Moura, M.; Goncalves, J.; Marques, A. & De Castro, P. (1997). Modeling compression failure after low velocity impact on laminated composites using interface elements. *Journal of Composite Materials*, Vol. 31, No. 15, 1462-1479
- De Xie, A. & Waas, A. (2006). Discrete cohesive zone model for mixed-mode fracture using finite element analysis. *Engineering Fracture Mechanics*, Vol. 73, No. 13, 1783-1796
- Gao, Y. & Bower, A. (2004). A simple technique for avoiding convergence problems in finite element simulations of crack nucleation and growth on cohesive interfaces. *Modelling and Simulation in Materials Science and Engineering*, Vol. 12, No. 3, 453-463
- Glennie, E. (1971). A strain-rate dependent crack model. *Journal of the Mechanics and Physics of Solids*, Vol. 19, No. 5, 255-272
- Goncalves, J.; De Moura, M.; De Castro, P. & Marques, A. (2000). Interface element including point-to-surface constraints for three-dimensional problems with damage propagation. *Engineering Computations*, Vol. 17, No. 1, 28-47
- Gustafson, P. & Waas, A. (2008). Efficient and robust traction laws for the modeling of adhesively bonded joints. *49th AIAA/ASME/ASCE/AHS/ASC Structures, Structural Dynamics, and Materials Conference*, pp. 1-16, April 2008, Schaumburg, IL, USA
- Hu, N.; Zemba, Y.; Okabe, T.; Yan, C.; Fukunaga, H. & Elmarakbi, A. (2008). A new cohesive model for simulating delamination propagation in composite laminates under transverse loads. *Mechanics of Materials*, Vol. 40, No. 11, 920-935
- Hu, N.; Zemba, Y.; Fukunaga, H.; Wang, H. & Elmarakbi, A. (2007). Stable numerical simulations of propagations of complex damages in composite structures under transverse loads. *Composite Science and Technology*, Vol. 67, No. 3-4, 752-765
- Kubair, D.; Geubelle, P. & Huang, Y. (2003). Analysis of a rate dependent cohesive model for dynamic crack propagation. *Engineering Fracture Mechanics*, Vol. 70, No. 5, 685-704
- LSTC, Livermore Software Technology Corporation, California, USA, LS-DYNA 970, 2005
- Mi, Y.; Crisfield, M. & Davis, G. (1998). Progressive delamination using interface element. *Journal of Composite Materials*, Vol. 32, No. 14, 1246-1272
- Morais, A.; Marques, A. & De Castro, P. (2000). Estudo da aplicacao de ensaios de fractura interlaminar de mode I a laminados compositos multidireccionais. *Proceedings of the 7as jornadas de fractura, Sociedade Portuguesa de Materiais*, p. 90-95, 2000, Portugal
- Moshier, M. (2006). Ram load simulation of wing skin-spar joints: new rate-dependent cohesive model. RHAMM Technologies LLC, USA, Report No. R-05-01
- Petrossian, Z. & Wisnom, M. (1998). Prediction of delamination initiation and growth from discontinues plies using interface elements. *Composite A*, Vol. 29, 503-515
- Pinho, S.; Iannucci, L. & Robinson, P. (2006). Formulation and implementation of decohesion elements in an explicit finite element code. *Composite A*, Vol. 37, 778-789
- Pinho, S.; Camanho, P. & De Moura, M. (2004). Numerical simulation of the crushing process of composite materials. *International Journal of Crashworthiness*, Vol. 9, No. 3, 263-76

- Reddy, E.; Mello, F. & Guess, T. (1997). Modeling the initiation and growth of delaminations in composite structures. *Journal of Composite Materials*, Vo. 31, No. 8, 812-831
- Riks, E. (1979). An incremental approach to the solution of snapping and buckling problems. *International Journal of Solid and Structures*, Vo. 15, 529-551
- Shahwan, K. & Waas, A. (1997). Non-self-similar decohesion along a finite interface of unilaterally constrained delaminations. *Proceeding of the Royal Society of London A*, Vol. 453, No. 1958, 515-550
- Tvergaard, V. & Hutchinson, J. (1996). Effect of strain-dependent cohesive zone model on predictions of crack growth resistance. *International Journal of Solid and Structures*, Vol. 33, No. 20-22, 3297-3308
- Xu, D.; Hui, E.; Kramer, E. & Creton, C. (1991). A micromechanical model of crack growth along polymer interfaces. *Mechanics of Materials*, Vol. 11, No. 3, 257-268

IntechOpen



Advances in Composite Materials - Ecodesign and Analysis

Edited by Dr. Brahim Attaf

ISBN 978-953-307-150-3

Hard cover, 642 pages

Publisher InTech

Published online 16, March, 2011

Published in print edition March, 2011

By adopting the principles of sustainable design and cleaner production, this important book opens a new challenge in the world of composite materials and explores the achieved advancements of specialists in their respective areas of research and innovation. Contributions coming from both spaces of academia and industry were so diversified that the 28 chapters composing the book have been grouped into the following main parts: sustainable materials and ecodesign aspects, composite materials and curing processes, modelling and testing, strength of adhesive joints, characterization and thermal behaviour, all of which provides an invaluable overview of this fascinating subject area. Results achieved from theoretical, numerical and experimental investigations can help designers, manufacturers and suppliers involved with high-tech composite materials to boost competitiveness and innovation productivity.

How to reference

In order to correctly reference this scholarly work, feel free to copy and paste the following:

Ahmed Elmarakbi (2011). Finite Element Analysis of Delamination Growth in Composite Materials using LS-DYNA: Formulation and Implementation of New Cohesive Elements, *Advances in Composite Materials - Ecodesign and Analysis*, Dr. Brahim Attaf (Ed.), ISBN: 978-953-307-150-3, InTech, Available from: <http://www.intechopen.com/books/advances-in-composite-materials-ecodesign-and-analysis/finite-element-analysis-of-delamination-growth-in-composite-materials-using-ls-dyna-formulation-and->

INTECH
open science | open minds

InTech Europe

University Campus STeP Ri
Slavka Krautzeka 83/A
51000 Rijeka, Croatia
Phone: +385 (51) 770 447
Fax: +385 (51) 686 166
www.intechopen.com

InTech China

Unit 405, Office Block, Hotel Equatorial Shanghai
No.65, Yan An Road (West), Shanghai, 200040, China
中国上海市延安西路65号上海国际贵都大饭店办公楼405单元
Phone: +86-21-62489820
Fax: +86-21-62489821

© 2011 The Author(s). Licensee IntechOpen. This chapter is distributed under the terms of the [Creative Commons Attribution-NonCommercial-ShareAlike-3.0 License](#), which permits use, distribution and reproduction for non-commercial purposes, provided the original is properly cited and derivative works building on this content are distributed under the same license.

IntechOpen

IntechOpen